

Sub-Kelvin optical thermometry of an electron reservoir coupled to a self-assembled InGaAs quantum dot

F. Seilmeier, M. Hauck, E. Schubert, G. J. Schinner, S. E. Beavan,* and A. Högele†
*Fakultät für Physik and Center for NanoScience (CeNS),
Ludwig-Maximilians-Universität München, Geschwister-Scholl-Platz 1, 80539 München, Germany*
(Dated: April 13, 2022)

We show how resonant laser spectroscopy of the trion optical transitions in a self-assembled quantum dot can be used to determine the temperature of a nearby electron reservoir. At finite magnetic field the spin-state occupation of the Zeeman-split quantum dot electron ground states is governed by thermalization with the electron reservoir via co-tunneling. With resonant spectroscopy of the corresponding excited trion states we map out the spin occupation as a function of magnetic field to establish optical thermometry for the electron reservoir. We demonstrate the implementation of the technique in the sub-Kelvin temperature range where it is most sensitive, and where the electron temperature is not necessarily given by the cryostat base temperature.

Self-assembled semiconductor quantum dots (QDs) represent promising building blocks for quantum information processing [1], and more recently have emerged as an intriguing model system for optical studies of the quantum impurity problem - the interaction of a localized electron with the continuum of states in a fermionic reservoir [2]. In the regime of strong tunnel coupling of a resident QD electron to the nearby Fermi sea and sufficiently low temperatures, signatures of many-body phenomena are observable in emission [3] or absorption with power-law tails characteristic of the Fermi-edge singularity [4] and the Kondo effect [5] in resonant spectra of neutral and singly charged QDs. In addition to resonant laser spectroscopy of charge-tunable QDs [6] and the control of their exchange coupling to the Fermi reservoir enabled by the gate voltage in QD field-effect devices [7], related experiments crucially require cryogenic temperatures deep in the sub-Kelvin regime [4, 5].

While the temperature of the electron reservoir is a key parameter in exploiting many-body phenomena, it is not necessarily the same as that of the cryogenic bath, and is difficult to access directly. In this Letter, we present a spectroscopic method to determine the electron bath temperature. Our technique exploits the sensitivity of spin-selective optical absorption in singly charged QDs [8–10] to temperature. A measurement of the effective QD electron spin temperature can be directly related to the spin bath temperature of the Fermi reservoir [11–13]. Although the QD-bath temperature relationship is complicated by optical spin pumping (OSP), in the limit of strong exchange coupling between the QD spin and the Fermi bath via co-tunneling, the OSP is negligible, and the QD spin state occupation is entirely governed by the thermal distribution of the electrons in the Fermi sea. In either case (with or without OSP), the QD electron spin polarization measured as a function of an external magnetic field provides a direct measure of the electron bath temperature.

In our experiment we used self-assembled InGaAs quantum dots grown by molecular beam epitaxy [14]

with intermediate annealing [15]. The QDs were embedded inside a field effect device [16] where a 25 nm thick GaAs tunneling barrier separates the QDs from a heavily n^+ doped GaAs layer that forms the Fermi reservoir. The QD-layer was capped subsequently by 10 nm GaAs, an AlGaAs/GaAs superlattice of 252 nm thickness, and 14 nm of GaAs. A semitransparent NiCr layer of 5 nm was evaporated on the surface to form the top electrode. A gate voltage applied to the top electrode tunes the QD energy levels relative to the Fermi level pinned in the back reservoir to control the QD charge occupation [17] and the exciton emission energy through the quantum confined Stark effect [18]. Moreover, the gate voltage also varies the coupling between the QD electron spin and the Fermi reservoir (given by the co-tunneling rate) by orders of magnitude [7].

The sample was mounted inside a ^3He refrigerator with a nominal minimum base temperature of $T_{\text{base}} = 250$ mK (Fig. 1a). The temperature was adjusted from 250 mK to 4.0 K by heating or pumping via the sorption pump on the ^3He pot. Optical access to the sample was provided by a fiber-based confocal microscope system with a spot size of $\approx 1 \mu\text{m}$ [19], addressing sufficiently few dots for single QD spectroscopy. We used the differential transmission method to address the neutral exciton (X^0) and trion (X^-) optical transitions in a single QD with resonant laser spectroscopy [6].

The evolution of the X^0 resonance with temperature is shown in Fig. 1b and c. Both fine-structure resonances of the neutral exciton exhibit a red-shift with increasing temperature (data points in Fig. 1b) consistent with a decrease of the band-gap energy in semiconductors described by the Varshni relation [20] (solid lines for bulk InAs and GaAs in Fig. 1b). The discrepancy between the measured resonance shift and the expected bulk values is not surprising given the uncertainty in both the material composition and the strain distribution inherent to self-assembled QDs. It also highlights the fact that a measurement of the resonance shift alone does not qualify as a reliable method for quantitative thermometry.

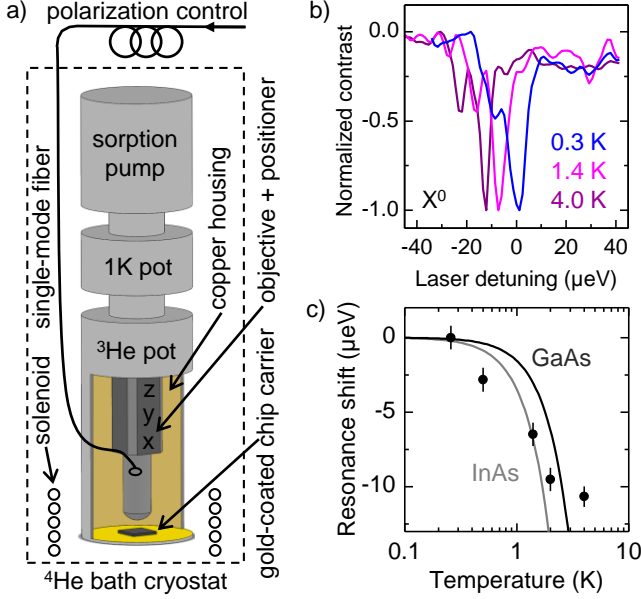


FIG. 1: (a) Experimental setup. The cryogenic system consists of a ^3He insert in a ^4He bath cryostat and provides a minimum base temperature of 250 mK. The solenoid is used to apply magnetic fields up to 10 T along the vertical axis of the cryostat. The quantum dot sample is mounted on a gold-coated chip carrier in thermal contact with the ^3He pot. Optical access to individual quantum dots is enabled with a fiber-based micro-objective mounted on an xyz nano-positioner. (b) Differential transmission spectra of the neutral exciton (X^0) transition at cryostat base temperatures $T_{\text{base}} = 0.3$ K, 1.4 K and 4.0 K show a resonance red-shift with increasing temperature. (c) The X^0 resonance shift as a function of T_{base} . The grey and black lines represent the temperature shift expected in bulk InAs and GaAs respectively.

Instead, we exploit the temperature dependence of the spin-resolved trion optical transitions in finite magnetic field [8, 9] to determine the electron bath temperature. The level diagram of the X^- in the presence of an optical drive at finite magnetic field applied in Faraday geometry is shown in Fig. 2a. The lower electron states with spin $\pm\frac{1}{2}$ (denoted as $|\uparrow\rangle = |1\rangle$ and $|\downarrow\rangle = |2\rangle$), and split by the electron Zeeman energy $\hbar\omega_Z^e = g_e\mu_B B$ couple to the trion states with two spin-singlet electrons and one heavy-hole with spin $\pm\frac{3}{2}$ (denoted as $|\uparrow\downarrow\uparrow\rangle = |4\rangle$ and $|\uparrow\downarrow\downarrow\rangle = |3\rangle$), and separated by the hole Zeeman energy $\hbar\omega_Z^h = g_h\mu_B B$. The dipole-allowed transitions between the blue ($|1\rangle - |4\rangle$) and red ($|2\rangle - |3\rangle$) Zeeman branches can be selectively addressed by σ^+ and σ^- circularly polarized laser fields with respective Rabi frequencies Ω_+ and Ω_- .

For strongly-confining QDs, the radiative decay rate Γ_0 is insensitive to magnetic field for realistic experimental field strengths and thus can be treated as equivalent for both dipole-allowed transitions. It also provides an upper bound on the dipole-forbidden diagonal transition rates

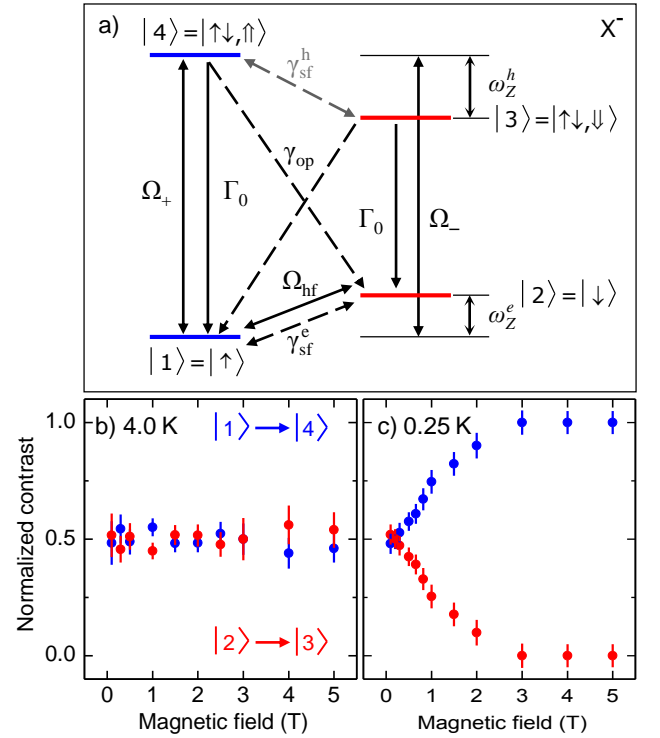


FIG. 2: (a) The four-level system associated with the X^- resonance in a charged QD, with a magnetic field applied in Faraday configuration. There are two dipole-allowed optical transitions associated with the upper $|1\rangle \leftrightarrow |4\rangle$ (blue transition) and lower $|2\rangle \leftrightarrow |3\rangle$ (red transition) Zeeman branches. The description of rates and Zeeman splittings is given in the text. (b) and (c) Normalized contrast for both the red and blue transitions measured as a function of magnetic field with $T_{\text{base}} = 4.0$ K and 250 mK, respectively. At large magnetic fields and a sufficiently low temperature the spin population accumulates in the spin-up ground state.

$\gamma_{\text{op}} = \eta\Gamma_0$ that become weakly allowed by heavy-hole light-hole admixing with $\eta \ll 1$ and contribute to OSP [11]. Although there is a temperature-dependence in the incoherent hole spin-flip rate γ_{sf}^h [10, 21, 22], this effect is rendered negligible by the much faster optical decay channel, i.e. $\gamma_{\text{op}} \gg \gamma_{\text{sf}}^h$. Another temperature insensitive parameter is the coherent coupling of the electron spin-states mediated by the hyperfine interaction with a ‘frozen’ nuclear spin environment. This leads to an effective coupling $\hbar\Omega_{\text{hf}} \sim 1 \mu\text{eV}$ [11, 23, 24], while the analogous coherent coupling of the excited states is negligible due to much weaker hole hyperfine interaction [25, 26]. Finally, since both the hyperfine-mediated and the spin-orbit induced spin-flip processes are negligible in our experiment as compared to the spin-exchange rate with the Fermi reservoir via co-tunneling (at a rate γ_{ct}), our inspection of the optically driven four-level system arrives at the conclusion that the only sensitivity to temperature stems from $\gamma_{\text{sf}}^e = \gamma_{\text{ct}}$. Importantly, the asymmetry

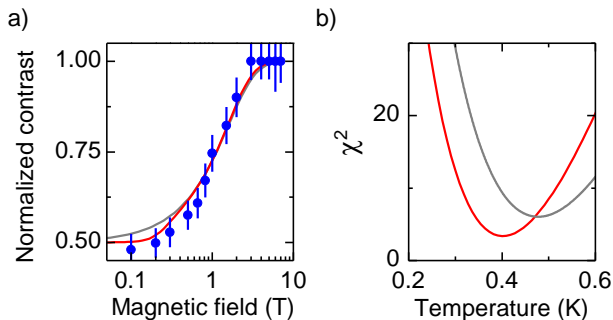


FIG. 3: (a) Normalized contrast measured at $T_{\text{base}} = 250$ mK, along with the temperature-fit results using the full four-level model described in the text (red line, $T_e = 400$ K), and the two-level thermal model (grey line, $T_e = 480$ K). (b) The mean-squared ‘distance’ between the data and the model predictions for the normalized contrast indicates a better fit by the four-level model (red line) as compared to the two-level thermal distribution (grey line).

between the ground state occupations in the absence of OSP has an exponential dependence on the temperature $\gamma_{12} = \gamma_{21} \exp(-\omega_Z^e/k_B T)$. This fact is exploited in the following to determine the electron bath temperature T_e with trion laser spectroscopy.

Experimentally, it is convenient to use linear polarization to address both trion transitions with one laser field scanned in frequency, and we chose $\Omega_+ = \Omega_- \simeq \Gamma_0$ to drive the transition close to saturation where the signal-to-noise ratio of the differential transmission contrast α is optimal [27]. Fig. 2b and c summarize the results obtained for the spin-resolved trion branches at different magnetic fields and temperatures. For finite magnetic fields, the two optical transitions were well resolved, and the peak amplitudes were used to calculate the normalized transmission contrast as $\alpha_{\text{blue,red}}/(\alpha_{\text{blue}} + \alpha_{\text{red}})$ for the blue and red transition accordingly.

The normalized contrasts in Fig. 2b and c correspond to nominal base temperatures of 4.0 K and 250 mK, respectively. While there is no significant evolution of the normalized contrast with magnetic field at 4.0 K, the relative strength of the blue transition grows at the expense of the red transition for the lowest temperature of our ${}^3\text{He}$ system. In this case, the normalized contrasts saturate for magnetic fields above 3 T, implying a negligible population of the state $|\downarrow\rangle$ and a spin accumulation in the $|\uparrow\rangle$ state. This asymptotic limit is expected for a thermal spin distribution in a singly charged QD governed by fast co-tunneling processes [8]. At moderate magnetic fields, however, the spin-state population is modified by optical spin-pumping [9] whenever $\gamma_{\text{ct}} \simeq \gamma_{\text{op}}$. In our sample with a nominal separation of 25 nm between the electron reservoir and the QD-layer, we estimate the tunnel coupling γ_t (see Fig. 4b) in the range between 10 μeV and

50 μeV for strongly confining QDs with emission around 1.3 eV. In the center of the trion stability plateau, the working point in our experiments, this implies a competition between effective thermal and optical spin-pumping rates at deep sub-Kelvin temperatures, necessitating a full four-level system analysis.

The four-level system is modelled using a Lindblad master equation, similarly to Ref. [10]. The Hamiltonian contains the coherent dynamics due to both optical fields Ω_+ and Ω_- with $\Omega_{\pm} = 2.5 \times \Gamma_0$, and the hyperfine term $\hbar\Omega_{\text{hf}} = 1.3 \mu\text{eV}$. The incident laser field also drives the weakly allowed off-diagonal transitions with Rabi frequencies of $\eta\Omega_{\pm}$, where we take $\eta \approx 4 \times 10^{-4}$ [11]. The incoherent transition rates; $\hbar\Gamma_0 = 1 \mu\text{eV}$, $\gamma_{\text{op}} = \eta\Gamma_0$, $\gamma_{21} = \gamma_{\text{ct}}$, and γ_{12} as defined above are included in the usual Lindblad superoperator formalism. The value of the co-tunneling rate at the minimum base temperature of 250 mK is estimated as $\hbar\gamma_{\text{ct}} \approx 5 \times 10^{-4} \mu\text{eV}$ [7]. An additional term is included to account for the broadening of the optical resonance that is caused by environmental charge and spin fluctuations [6, 28]; in our experiments the observed resonance width was $\hbar\Gamma \approx 6 \mu\text{eV}$ (Fig. 1b). We include the effect as pure dephasing of the excited states with a rate of $\Gamma_d/2 = 2.5 \mu\text{eV}$ that contributes to the experimental linewidth as $\Gamma = \Gamma_0 + \Gamma_d$. The electron and hole g -factors are taken as $g_e = 0.69$ and $g_h = 0.81$ [12]. The steady-state solutions for the density matrix are found numerically [29], for both cases when the red and blue transitions are driven resonantly. The normalized absorption contrast is calculated using the relevant coherence terms of the density matrix.

The model is used to fit the data recorded at $T_{\text{base}} = 250$ mK with the temperature as the only free parameter. The optimized fit gives a value of $T_e = 400 \pm 50$ mK. The solution of the four-level model is shown in Fig. 3a, along with the result expected from a thermal population distribution between the two ground states. As expected for this low value of γ_{ct} in our sample in the sub-Kelvin regime, there is evidence of optically induced spin pumping at low magnetic field values (< 500 mT), where the normalized contrasts remain closer to 0.5 (i.e. equal population in both states $|1\rangle$ and $|2\rangle$) than would be expected in a purely thermodynamic equilibrium. The four-level model qualitatively captures this spin pumping trend, and therefore provides a better fit as compared to the two-level model (see Fig. 3b). The temperature determined by the four-level model fit changes by less than 10% with variations in the values of η and Ω_{hf} by a factor of 2, or an order of magnitude change in γ_{ct} . In contrast, the model is more sensitive to the values of Γ_0 , Ω_{\pm} and $g_{e,h}$.

For a general application of this thermometry method in alternate QD systems, it would be desirable to eliminate this OSP signature, and recover a simple two-level thermal system. We suggest two straightforward alterations that would allow for this simplification. Firstly,

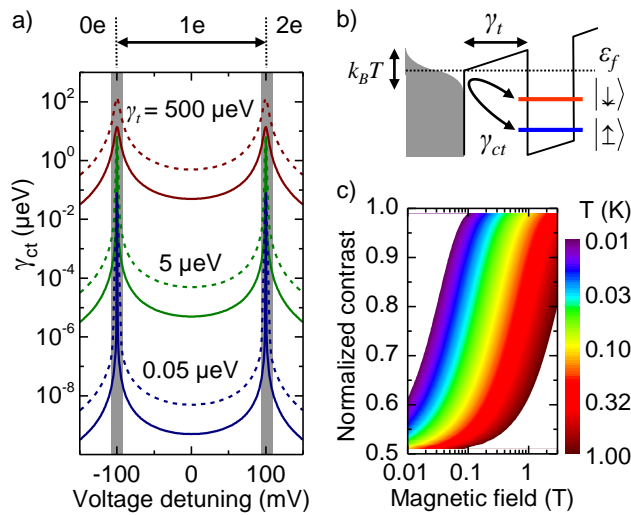


FIG. 4: (a) Optimal working regions for optical thermometry of the electron reservoir at the edges of the charge stability plateau are shaded grey. The co-tunneling rate γ_{ct} is plotted as a function of gate voltage detuning from the plateau center for 400 mK and 40 mK as dashed and solid lines according to Ref. [7]. (b) At the edges, the co-tunneling rate between the quantum dot electron states and the Fermi edge ϵ_F thermally broadened by $k_B T$ is maximum for a sample-specific tunnel coupling γ_t (500 μeV , 5 μeV and 0.05 μeV roughly correspond to tunneling barriers of 15 nm, 25 nm, and 35 nm). Tuning to the maximum γ_{ct} simplifies the system dynamics to an effective thermal two-level system, and a single measurement of the normalized contrast at a particular applied magnetic field should suffice to determine the temperature of the electron reservoir using the color-map shown in (c).

the effectiveness of optically induced spin pumping could be reduced by pumping with circularly rather than linearly polarized light such that only one of the optical transitions is driven efficiently at small magnetic fields. Secondly, the relaxation rate γ_{ct} can be increased relative to the optical spin-pumping channel, given by rates Ω_{\pm} and γ_{op} . The value of γ_{ct} can be controllably tuned across a few orders of magnitude by varying the gate-voltage, and can be further altered for different samples by tailoring the tunnel barrier energy itself. Fig. 4a shows how the co-tunneling rate varies with gate voltage for a number of different tunnel-barrier energies, and also for different temperatures [7]. It will in most cases be possible to increase γ_{ct} sufficiently by tuning the gate voltage (shaded regions in Fig. 4a), and move into an elegantly simple regime where the normalized contrast directly reflects a thermal distribution in a two-level system.

Another mechanism through which the system dynamics will significantly deviate from that of a two-level thermal distribution could arise due to the dynamic interaction between the electron spin and the 10^5 nuclear spins in the QD [30]. The effect known as dragging

(anti-dragging) occurs when the electron-spin causes the nuclear-spins to align in such a way as to Zeeman-shift the transition into (out of) resonance with the incident light [31, 32]. This effect is particularly pronounced at high magnetic fields, long integration times, and when the step-size of the laser frequency sweep is small. In the current experiment, dragging effects were minimized by choosing a large laser step-size. An alternative method to eliminate nuclear spin magnetization would be to actively depolarize the nuclear spin ensemble [33].

If the experimental conditions are chosen such that the two-level approximation is valid, then the electron reservoir temperature T_e can be read out with a single normalized-contrast measurement using the colormap shown in Fig. 4c. To quantify the precision of this method in determining the temperature, we use the best-case signal to noise ratios achievable with either differential transmission measurements (6×10^3 using a GaAs solid immersion lens [34]) or resonance fluorescence (10^5 , [28]). This results in a temperature measurement with uncertainty as low as 0.004 % using resonance fluorescence, or 0.06 % with differential transmission spectroscopy. Therefore this method could potentially measure mK temperatures with sub- μK precision.

In conclusion, we have developed and demonstrated a novel technique to determine the temperature of an electron spin bath. This was achieved by optically driving a QD tunnel-coupled to the electron spin bath, and monitoring its spin polarization as a function of magnetic field. At mK temperatures, the actual temperature of the electron reservoir can deviate significantly from the nominal base temperature of the cryostat, as was the case here where the temperature was determined as 400 ± 50 mK at a cryostat base temperature of 250 mK. By maximizing the co-tunneling rate γ_{ct} via the gate-voltage, the four-level system description simplifies to a two-level thermal system, allowing for a straightforward and simple method of electron bath thermometry. The sensitivity of this method is optimal at low temperatures ($T < 1$ K). The parameter range of low temperatures and large co-tunneling rates coincides with the regime of interest for exploring the many-body interactions between a QD and an electron bath, where the reservoir temperature is an important parameter. Thus, the optical thermometry technique will be a particularly useful tool in future investigations of many-body phenomena in self-assembled QD systems.

We acknowledge A. Badolato and P. M. Petroff for growing the sample heterostructure used in this work, and M. Kroner for useful discussions. This research was funded by the Deutsche Forschungsgemeinschaft (SFB 631 and the German Excellence Initiative via the Nanosystems Initiative Munich, NIM) with support from the Center for NanoScience (CeNS) and LMUexcellent.

-
- * Electronic address: sarah@beavan.com.au
 † Electronic address: alexander.hoegele@lmu.de
- [1] A. Imamoğlu, H. Schmidt, G. Woods, and M. Deutsch, *Phys. Rev. Lett.* **79**, 1467 (1997).
- [2] H. E. Türeci, M. Hanl, M. Claassen, A. Weichselbaum, T. Hecht, B. Braunecker, A. O. Govorov, L. Glazman, A. Imamoğlu, and J. von Delft, *Phys. Rev. Lett.* **106**, 107402 (2011).
- [3] N. A. J. M. Kleemans, J. van Bree, A. O. Govorov, J. G. Keizer, G. J. Hamhuis, R. Nötzel, A. Y. Silov, and P. M. Koenraad, *Nature Phys.* **6**, 534 (2010).
- [4] F. Haupt, S. Smolka, M. Hanl, W. Wüster, J. Miguel-Sanchez, A. Weichselbaum, J. von Delft, and A. Imamoğlu, *Phys. Rev. B* **88**, 161304 (2013).
- [5] C. Latta, F. Haupt, M. Hanl, A. Weichselbaum, M. Claassen, W. Wuester, P. Fallahi, S. Faelt, L. Glazman, J. von Delft, et al., *Nature* **474**, 627 (2011).
- [6] A. Högele, S. Seidl, M. Kroner, K. Karrai, R. J. Warburton, B. Gerardot, and P. M. Petroff, *Phys. Rev. Lett.* **93**, 217401 (2004).
- [7] J. Smith, P. Dalgarno, R. J. Warburton, A. O. Govorov, K. Karrai, B. Gerardot, and P. M. Petroff, *Phys. Rev. Lett.* **94**, 197402 (2005).
- [8] A. Högele, M. Kroner, S. Seidl, K. Karrai, M. Atatüre, J. Dreiser, A. Imamoğlu, R. J. Warburton, A. Badolato, B. D. Gerardot, et al., *App. Phys. Lett.* **86**, 221905 (2005).
- [9] M. Atatüre, J. Dreiser, A. Badolato, A. Högele, K. Karrai, and A. Imamoğlu, *Science* **312**, 551 (2006).
- [10] B. D. Gerardot, D. Brunner, P. A. Dalgarno, P. Ohberg, S. Seidl, M. Kroner, K. Karrai, N. G. Stoltz, P. M. Petroff, and R. J. Warburton, *Nature* **451**, 441 (2008).
- [11] J. Dreiser, M. Atatüre, C. Galland, T. Müller, A. Badolato, and A. Imamoğlu, *Phys. Rev. B* **77**, 075317 (2008).
- [12] M. Kroner, K. Weiss, B. Biedermann, S. Seidl, A. Holleitner, A. Badolato, P. M. Petroff, P. Ohberg, R. J. Warburton, and K. Karrai, *Phys. Rev. B* **78**, 075429 (2008).
- [13] C. Latta, A. Srivastava, and A. Imamoğlu, *Phys. Rev. Lett.* **107**, 167401 (2011).
- [14] D. Leonard, M. Krishnamurthy, C. M. Reaves, S. P. Denbaars, and P. M. Petroff, *App. Phys. Lett.* **63**, 3203 (1993).
- [15] J. M. Garcia, G. Medeiros-Ribeiro, K. Schmidt, T. Ngo, J. L. Feng, A. Lorke, J. P. Kotthaus, and P. M. Petroff, *App. Phys. Lett.* **71**, 2014 (1997).
- [16] H. Drexler, D. Leonard, W. Hansen, J. P. Kotthaus, and P. M. Petroff, *Phys. Rev. Lett.* **73**, 2252 (1994).
- [17] R. J. Warburton, C. Schaflein, D. Haft, F. Bickel, A. Lorke, K. Karrai, J. M. Garcia, W. Schoenfeld, and P. M. Petroff, *Nature* **405**, 926 (2000).
- [18] R. J. Warburton, C. Schulhauser, D. Haft, C. Schäflein, K. Karrai, J. M. Garcia, W. Schoenfeld, and P. M. Petroff, *Phys. Rev. B* **65**, 113303 (2002).
- [19] A. Högele, S. Seidl, M. Kroner, K. Karrai, C. Schulhauser, O. Sqalli, J. Scrimgeour, and R. J. Warburton, *Rev. Sci. Instrum.* **79**, 023709 (2008).
- [20] Y. P. Varshni, *Physica* **34**, 149 (1967).
- [21] D. Brunner, B. D. Gerardot, P. A. Dalgarno, G. Wüst, K. Karrai, N. G. Stoltz, P. M. Petroff, and R. J. Warburton, *Science* **325**, 70 (2009).
- [22] J. Houel, A. V. Kuhlmann, L. Greuter, F. Xue, M. Poggio, B. D. Gerardot, P. A. Dalgarno, A. Badolato, P. M. Petroff, A. Ludwig, et al., *Phys. Rev. Lett.* **108**, 107401 (2012).
- [23] A. Bracker, E. Stinaff, D. Gammon, M. Ware, J. Tischler, A. Shabaev, A. Efros, D. Park, D. Gershoni, V. Korenev, et al., *Phys. Rev. Lett.* **94**, 047402 (2005).
- [24] P.-F. Braun, X. Marie, L. Lombez, B. Urbaszek, T. Amand, P. Renucci, V. Kalevich, K. Kavokin, O. Krebs, P. Voisin, et al., *Phys. Rev. Lett.* **94**, 116601 (2005).
- [25] P. Fallahi, S. T. Yilmaz, and A. Imamoğlu, *Phys. Rev. Lett.* **105**, 257402 (2010).
- [26] E. A. Chekhovich, M. N. Makhonin, K. V. Kavokin, A. B. Krysa, M. S. Skolnick, and A. I. Tartakovskii, *Phys. Rev. Lett.* **104**, 066804 (2010).
- [27] B. D. Gerardot, S. Seidl, P. A. Dalgarno, R. J. Warburton, M. Kroner, K. Karrai, A. Badolato, and P. M. Petroff, *App. Phys. Lett.* **90**, 221106 (2007).
- [28] A. V. Kuhlmann, J. Houel, A. Ludwig, L. Greuter, D. Reuter, A. D. Wieck, M. Poggio, and R. J. Warburton, *Nature Phys.* **9**, 570 (2013).
- [29] J. Johansson, P. Nation, and F. Nori, *Comput. Phys. Commun.* **184**, 1234 (2013).
- [30] B. Urbaszek, X. Marie, T. Amand, O. Krebs, P. Voisin, P. Maletinsky, A. Högele, and A. Imamoğlu, *Rev. of Modern Phys.* **85**, 79 (2013).
- [31] A. Högele, M. Kroner, C. Latta, M. Claassen, I. Carusotto, C. Bulutay, and A. Imamoğlu, *Phys. Rev. Lett.* **108**, 197403 (2012).
- [32] W. Yang and L. J. Sham, *Phys. Rev. B* **85**, 235319 (2012).
- [33] E. A. Chekhovich, K. V. Kavokin, J. Puebla, A. B. Krysa, M. Hopkinson, A. D. Andreev, A. M. Sanchez, R. Beanland, M. S. Skolnick, and A. I. Tartakovskii, *Nature Nanotech.* **7**, 646 (2012).
- [34] A. N. Vamivakas, M. Atatüre, and J. Dreiser, *Nano Letters* **7**, 2892 (2007).